

pubs.acs.org/JPCA Article

The Role of Ion Rotation in Ion Mobility: Ultrahigh-Precision Prediction of Ion Mobility Dependence on Ion Mass Distribution and Translational to Rotational Energy Transfer

Christopher P. Harrilal,* Sandilya V.B Garimella, Jaehun Chun, Nikhil Devanathan, Xueyun Zheng, Yehia M Ibrahim, Carlos Larriba-Andaluz, Gregory Schenter, and Richard D. Smith



Cite This: J. Phys. Chem. A 2023, 127, 5458-5469



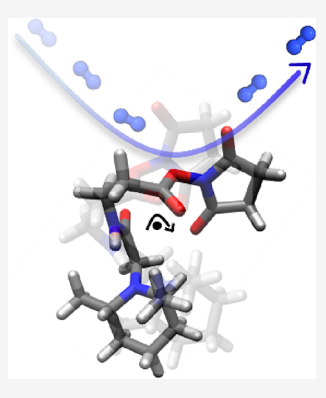
ACCESS I

III Metrics & More

Article Recommendations

Supporting Information

ABSTRACT: The role of ion rotation in determining ion mobilities is explored using the subtle gas phase ion mobility shifts based on differences in ion mass distributions between isotopomer ions that have been observed with ion mobility spectrometry (IMS) measurements. These mobility shifts become apparent for IMS resolving powers on the order of ~1500 where relative mobilities (or alternatively momentum transfer collision cross sections; Ω) can be measured with a precision of ~10 ppm. The isotopomer ions have identical structures and masses, differing only in their internal mass distributions, and their Ω differences cannot be predicted by widely used computational approaches, which ignore the dependence of Ω on the ion's rotational properties. Here, we investigate the rotational dependence of Ω , which includes changes to its collision frequency due to thermal rotation as well as the coupling of translational to rotational energy transfer. We show that differences in rotational energy transfer during ion—molecule collisions provide the major contribution to isotopomer ion separations, with only a minor contribution due to an increase in collision frequency due to ion rotation. Modeling including these factors allowed for differences in Ω to be calculated that precisely mirror the experimental separations. These findings also highlight



the promise of pairing high-resolution IMS measurements with theory and computation for improved elucidation of subtle structural differences between ions.

1. INTRODUCTION

Ion mobility spectrometry (IMS) separates gas phase ions as they move though a gas under the influence of an electric field. Image is often coupled to mass spectrometry (MS), allowing for ion mobility and mass-to-charge (m/z) measurements to be made simultaneously, and the combination has been employed in areas of physical and analytical chemistry, which include gas phase structural biology, the chemical kinetics, some separations, $^{10-12}$ molecular class identifications, and broad "omics" measurements. The mobility (K) of an ion under equilibrium subject to an electric field (E) is given by eq 1:

$$K = \frac{v_d}{E} \tag{1}$$

where ν_d is the net ion relative velocity through the gas in a steady-state condition. The drift velocity of an ion is dependent on the experimental conditions such as the pressure, temperature, and gas identity. The mobility of an ion is often related to its momentum transfer cross section (Ω) (often incorrectly referred to as a collision cross section) via Mason—Schamp's equation (Ω)

$$\Omega = \frac{3}{16} \sqrt{\frac{2\pi}{\mu k_b T}} \frac{ze}{N_0 K_0} \tag{2}$$

Here, μ is the reduced mass $(\mu = \frac{m_a \times m_b}{m_a + m_b})$ of the colliding partners (i.e., ion a and gas b), k_b is Boltzmann's constant, T is the buffer gas temperature, z is the ion charge, e is the elementary charge, N_0 is Loschmidt's number representing the number density of gas at standard conditions, and K_0 is the reduced mobility, $K_o = K\left(\frac{N}{N_o}\right)$, used to normalize for experimental conditions, where N is the gas number density at the measured pressure and temperature.

Ion mobility can be used to help identify compounds of known mobility as well as previously unknown or unsuspected compounds using calculated mobilities for plausible structures. In general, an agreement of 1–3% between a measured and predicted Ω value is considered acceptable and not unreasonable based on the previously low experimental resolving powers. The utility of this approach increases with improvements to both the accuracy and precision of IMS

Received: February 24, 2023 Revised: May 12, 2023 Published: June 18, 2023





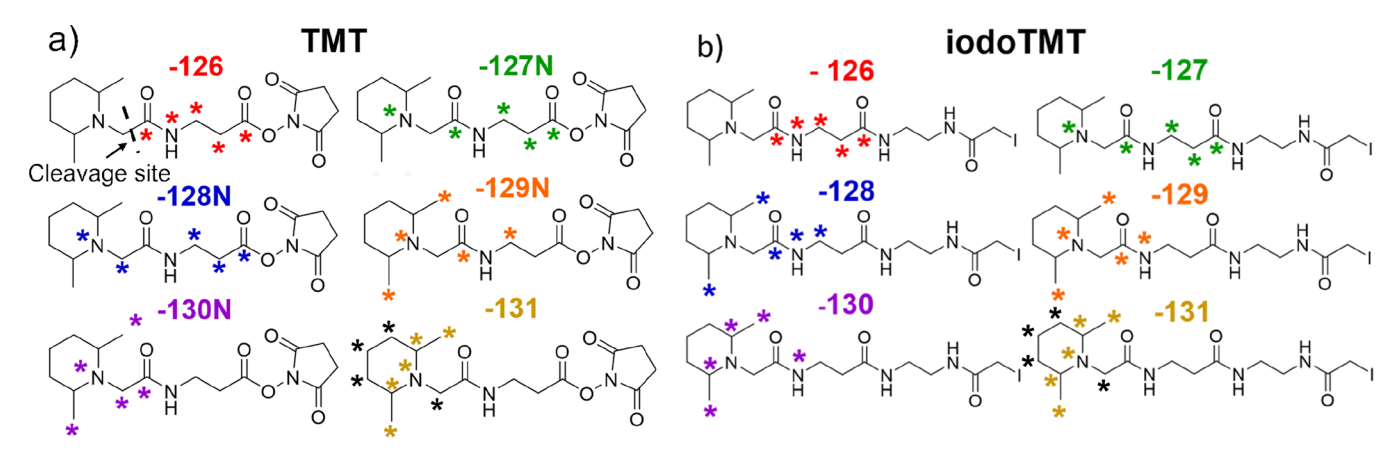


Figure 1. 2D structures of isotopomers -126 to -131 of (a) TMT and (b) iodoTMT. Each isotopomer contains 5 heavy atom substitutions, four 13 C, and one 15 N, and the placement of the heavy labels is indicated with asterisks. After separations, collisional activation of these isotopomer ions yields 'reporter' fragment ions, allowing them to be distinguished. The dominant cleavage site upon collisional activation is identical between all isotopomers and is indicated for TMT-126. Cleavage at this site for the -126 isotopomer results in a reporter ion of m/z 126. Black asterisks on the -131 isotopomers represent the locations of the $[M+1]^+$ isotopologue of the -131 isotopomer, which results in a reporter ion m/z 132.

 Ω measurements. The resolving power in traditional drift tube ion mobility spectrometry (DTIMS) experiments is limited by the practical constraints associated with increasing the path length of the separation, electric field strength, and pressure. 19 Techniques such as traveling-wave ion mobility (TWIMS) however have demonstrated the ability to overcome limitations associated limited path length as ions are moved using low amplitude traveling waves rather than relying on a constant electric field gradient through the mobility device.²⁰ In particular, SLIM utilize large arrays of electrodes on two planar evenly spaced surfaces (e.g., printed circuit boards) spaced by ~3 mm. ²¹ The electrodes are organized in a manner such that the application of RF, DC, and TW potentials allow for ion confinement and motion through extremely long serpentine paths. The displacement of an ion along the path by the traveling waves is dependent on its mobility, where ions of high mobility are displaced to a larger degree while lower mobility ions to a lesser degree. SLIM can also pass ions several times through the device with minimal signal loss, allowing for ultrahigh-resolution separation. 20-22 The improvements in IMS resolving power using TW-SLIM²⁰⁻²² have allowed ions with very subtle mobility differences, <0.005% (50 ppm), to be separated. A striking example recently reported is the mobility differences for isotopomers, ²³ isotopic isomer ions having identical structures, masses, and numbers of each nuclide (differing only in their locations, e.g., C_{12} vs C_{13}). These mobility shifts have been attributed to the isotopomer mass distribution differences that change the ion's center of mass (CoM) and thus impact the ion's moment of inertia (MoI) and collisional energy transfer. 23,24 The mobility differences observed are on the order of ~10-450 ppm and representative of recent gains in IMS resolving powers. More recently, additional mobility shifts have been reported for conformations of vitamin D and positional isomers of dibromoanilines and dichloroanilines and have been suggested to arise from similar mass distribution-based mobility effects.²⁵

The quality of IMS measurements now explicitly challenges computational capabilities for either accurately predicting mobilities or Ω values or precisely predicting the small differences in relative Ω between structurally similar isomers. The ability to distinguish compounds more confidently based upon small differences in their relative mobilities would have

significant utility, e.g., for more confident identification of isomers where no authentic standard is available. As an example, no present simulation approach we are aware of accounts for the mobility separation of isotopomer ions except for the very recently developed IMoS 2, which requires considerable computational resources. 24,26 The most accepted method of calculating Ω is through the trajectory method (TM),²⁷ where the collision integral is calculated using highly realistic ion-gas interactions. However, common assumptions made in the calculation of Ω ultimately limit their accuracy and precision. These assumptions include maintaining identical ion and buffer gas temperatures, incomplete descriptions of the interaction potentials, elastic collisions, etc. 28-30 While efforts have been made to explicitly consider such factors, ²⁸⁻³¹ the previously limited IMS resolving powers justified neglecting such contributions.

In this work, we investigate the role of ion rotation on Ω by considering two factors that are generally ignored: (i) the dependence of collision frequency due to the ion's rotation and (ii) the momentum transfer to the ion's rotational degrees of freedom during a collision. In regard to the first factor, when the rotational speed is comparable or faster than the timescale of collisions, an ion can manifest a greater collisional frequency than its non-rotating counterpart, as noted by Shvartsburg et al., ³² resulting in an increase in Ω . Shvartsburg *et al.* considered the consequences of the 'blurring' due to an ion's rotation (analogous to the increased effective area of a rotating propeller) that leads to an increase in collisional cross sections for all non-spherical ion structures. While isotopomers are structurally identical and have similar overall angular velocity distributions and, e.g., the same degree of "elongation", small differences in their mobilities or Ω could result from different collision frequencies arising from this blurring effect due to their different CoMs and rotational speeds.²³ The second factor is related to the inelasticity of collisions. Present computational approaches ignore energy partitioning to the ion's rotational (and vibrational) degrees of freedom. The partitioning of energy to these modes can influence the magnitude of momentum transfer between the collision partners.³² In the case of isotopomers, their differences in mass distribution and thus their MoI may influence how the gas interacts with structures of identical geometries.

Isotopomers provide an ideal case to investigate these effects as their 3D ion structures are identical but have small differences in their different CoM (and thus their rotational properties, i.e., the ion CoM about which they rotate and their MoI); all other parameters potentially affecting Ω calculations can be assumed identical for a set of isotopomers. In this work, we show that the mobility differences observed for isotopomer ions are largely a result of differences in energy transfer to rotational modes and not just differences in collision frequency. This allowed us to develop a more efficient computational approach accounting for Ω differences ≤50 ppm with little to no increase in computational burden compared to traditional approaches. This work provides a foundation for further development of high-precision Ω predictions of potential utility for distinguishing isomer and conformer ions using high-precision mobility measurements.

2. METHODS

2.1. Experimental Measurements. The experimental measurements for the mobilities the two isotopomer ion sets have been previously reported.²³ Briefly, a Structures for Lossless Ion Manipulations (SLIM) IMS coupled to mass spectrometry (MS) was used to carry out the mobility separations for sets of TMT and iodoTMT isotopomers (six each, designated as -126 through -131 based upon the mass of the reporter ion), see Figure 1, obtained from Thermo Fisher Scientific, Waltham, MA. The isotopomers of a given set (TMT or iodoTMT), 10 μ M each, in 50/50 water/methanol and 0.5% acetic acid, were electrosprayed to form the ions studied in SLIM-IMS separations using 1.5 torr N2 and traveling waves at 300 m/s with 27 V amplitude (0-peak) for TMT and 400 m/s at 35 V (0-peak) for iodoTMT. The ultrahigh resolution SLIM IMS separations used 100 passes, or \sim 1350 m pathlength. The individual TMT (m/z 345) and iodoTMT (m/z) 458) isotopomers were distinguished from one another post-IMS separation via fragmentation that provided 6 reporter ions of m/z 126-131, each unique to an isotopomer.²³ Measurements were performed in triplicate. The average arrival time differences in ppm for isotopomers -127 to -131 relative to -126 are provided in Table S1. The uncertainty is represented as the standard deviation of the relative difference in arrival time taken from triplicate measurements. The arrival times of the [M + 1] + isotopologue (m/z 346 and 459 for TMT and iodoTMT) for the -131 isotopomers are also provided relative to the arrival time of -126.

Separations performed using TW-IMS separations require the arrival time of unknown analyte ions to be calibrated based upon the arrival times of known ions with accepted Ω values. This calibration strategy is generally straight forward to implement in most experiments. However, to establish a calibrated mobility scale over the narrow mobility window, which the isotopomers span, estimated to be <0.05% of the full range due to the extensive multi-pass use for separations and limited mobility range before lapping occurs, would require calibrants of known mobilities that have only slightly higher and lower mobilities than the isotopomers being separated such that they are transmitted with the isotopomers within the same mobility window. Obtaining such calibrants with highly similar mobilities presents a significant challenge. Furthermore, the mobility of the calibrants would need to be accurately known to be useful. Devices such as drift tubes, where the mobility of an ion can be linearly correlated to its drift time, fail

to provide the required accuracy of mobility measurements for such separations.

One approach to address this would be to simply use the range of arrival times, but this is not completely satisfactory for the case of traveling wave-based separations. Thus, we have chosen an alternative; we estimate the relative magnitude of the mobility differences between the isotopomers. For this, we leverage the arrival time difference between the -131isotopomers and their [M + 1] + isotopologues (m/z) 346 and 459 for TMT and iodoTMT). The [M + 1] + isotopologue of the TMT and iodoTMT isotopomers is in itself a mixture of isotopomers in which the naturally occurring ¹³C can be on any non-labeled carbon. Activation of the [M + 1] + isotopologue, however, results in the production of a reporter ion (fragment) of m/z 132 that has an additional ¹³C on one of the sites indicated with a black asterisks in Figure 1. From this work, it is clear that the mobility shifts between isotopomers are influenced by their rotational differences, which indicates that the separation of the -131 isotopomer and its [M + 1] + isotopologue will be influenced by the change in mass as well as their difference in rotational properties. For reference, the arrival time difference between the [M + 1] + isotopologue of -131 and the -131 isotopomer is 125 ± 18 ppm and 224 ± 16 ppm for TMT and iodoTMT. The magnitude of this separation is about half the maximum separation between the lowest and highest mobility isotopomers of their respective sets. Thus, the changes in rotational properties can have a similar magnitude of influence on mobility differences as an increase in mass by 1 amu for ions of these sizes.

By ignoring the dependence of Ω on the rotational properties of an ion, one can use eq 2 to calculate the expected mobility differences based on the difference in reduced mass between the -131 isotopomer and its [M+1] + isotopologue. Based on the reduced mass differences alone, the [M+1] + isotopologue of -131 is expected to have and increase in Ω of 108 ppm for TMT and 66 ppm for iodoTMT. Taking the quotient of the arrival time difference between the -131 isotopomer and its [M+1] + isotopologue in ppm, one can establish a scale factor that relates the difference in arrival time to differences in Ω see eq 3:

scale factor =
$$\frac{t_{[M+1]^+\text{isotopologue of}-131} - t_{-131 \text{ isotopomer}}}{\text{calculated } \Omega \text{ difference based on reduced mass}}$$
(3)

The quotient of the relative arrival times of the isotopomers to -126 (Table S1) and the established scale factor can then be taken to establish an estimate of the magnitude of the relative mobility differences between isotopomers as is shown in eq 4:

Estimated Relative Mobility (ppm) =
$$\frac{t_{-1xx} - t_{-131}}{\text{scale factor}}$$
 (4)

This approach yields a lower bound on the relative magnitude of the Ω differences where the contribution of rotational properties to the arrival time differences are ignored. The estimated relative Ω differences using this approach are provided in Table 1.

The mobility for the TMT and iodoTMT isotopomers were measured on an Agilent 6560 Ion Mobility Q-ToF mass spectrometer. Drift times of Agilent tuning mix ions as well as TMT and iodoTMT were measured at an electric field

Table 1. Estimated Relative Ω Differences Based on Established Scale Factor (See Text for Details)

isotopomer	relative Ω^a (ppm)
TMT-126	0
TMT-127	13 ± 2
TMT-128	33 ± 15
TMT-129	171 ± 34
TMT-130	143 ± 28
TMT-131	257 ± 44
iodoTMT-126	0
iodoTMT-127	5 ± 1
iodoTMT-128	66 ± 2
iodoTMT-129	75 ± 2
iodoTMT-130	110 ± 4
iodoTMT-131	115 ± 3
^a Relative to −126 isotopomer	

strength of 1.85 V/cm. Ω calibration was performed via a linear fit of the reduced cross section of the Agilent tuning mix ions (CCS obtained from Stow *et al.*³³) vs their drift times.

2.2. Ion Conformational Selection. Conformational searching was preformed using the Monte Carlo multiple minimum method (MCMM) and OPLS3 forcefield in the MACROMODEL software package.³⁴ The resulting structures were optimized using DFT at the B3LYP/6-31+G* level of theory^{35,36} with Grimme's empirical dispersion correction (GD3BJ)³⁷ using Gaussian16.³⁸ Structures were ranked in terms of their Gibbs Free Energy at 298.15 K. A snapshot of the global minimum structure for TMT and iodoTMT is shown in Figure S1. All Ω calculations performed for the TMT and iodoTMT isotopomers in this work used the lowest energy geometry in terms of Gibbs free energy at 298.15 K since it closely resembles other low energy structures. While at room temperature there will be a distribution of structures present for a given ion, we expect that this likely does not affect the prediction of the relative differences in Ω , and we plan to study the conformation dependence of the isotopomer ions in a

2.3. Theoretical Approach and Simulations. A computational approach was developed, which accounts for the dependence of the rotationally averaged value of Ω on the rotational properties of the ion. Generally, the $\Omega_{\rm avg}$ is calculated using eq 5:

$$\Omega_{\text{avg}} = \frac{1}{4\pi^2} \int_0^{2\pi} d\theta \times \int_0^{\pi} d\varphi \sin \varphi \times \int_0^{2\pi} d\gamma \frac{\pi}{8} \left(\frac{\mu}{k_b T}\right)^3 \times \int_0^{\infty} dg e^{-\mu g^2/2k_b T} g^5 \times \int_0^{\infty} db 2b (1 - \cos \chi(\theta, \varphi, \gamma, g, b, I)) \tag{5}$$

where θ , φ , and γ represent the Euler angles that define the orientation of the molecule, g and μ represent the relative speed and reduced mass of the colliding partners, b is the impact parameter, and χ is the scattering angle.³ Modifications to eq S in this work come by adding the dependence of χ on the MoI by sampling the rotational speed (ω) distribution of the ion, during the course of the trajectory, such that the

deflection angles and collision frequency are sensitive to the ion's MoI (I) and rotational temperature ($T_{\rm R}$), as discussed below. As such, while eq 5 is derived assuming only elastic collisions, we expect that the effect of energy transfer on the scattering will be sufficient to provide a relative shift in the momentum transfer cross section, and thus the overall effect of inelasticity is discarded for the time being. The gas—ion interactions are described using 6-12 Lennard-Jones (LJ) potentials³⁹ along with a charge-induced dipole term (eq 6)

$$\Phi(r) = 4\sum_{i}^{N} \varepsilon_{i} \left[\left(\frac{\sigma_{i}}{r_{i}} \right)^{12} - \left(\frac{\sigma_{i}}{r_{i}} \right)^{6} \right] - \frac{\alpha}{2} \left(\frac{ze}{n} \right)^{2} \left[\left(\sum_{i}^{n} \frac{x_{i}}{r_{i}^{3}} \right)^{2} + \left(\sum_{i}^{n} \frac{y_{i}}{r_{i}^{3}} \right)^{2} + \left(\sum_{i}^{n} \frac{z_{i}}{r_{i}^{3}} \right)^{2} \right]$$

$$(6)$$

Here, r_i is the vector distance from the gas molecule to the *i*th atom (N atoms total), σ_i is the van der Waals radius of the ith atom, and ε_i is the depth of potential well of the *i*th atom, with values for specific atoms² given in Table S2, α is the gas polarizability (1.7 Å³ for N₂), and x_i , y_i , and z_i are the relative position of each individual atom. To validate the global minimum geometries used in this work, the experimentally measured Ω values are compared to the calculated Ω values when modeling the potential as described by eq 6 and employing the T- ε collision model (described in detail below). Note that additional terms can be added to eq 6 to account for additional interactions between N2 and the ion such as the ion-quadrupole interaction and the orientation of the linear N₂ molecule. These interactions can be important for very small ions and are thus ignored when calculating the absolute Ω values of the global minimum TMT and iodoTMT structures. Regarding the evaluation of Ω 's dependence on linear to rotational energy transfer, we model the potential by only accounting for the contribution due to the Lennard-Jones potentials and ignore the charge induced dipole term in eq 6. This is done for computational speed and due to the fact that we are working with isotopomers, which are identical in 3D structure. As such, we expect these terms to be identical between isotopomers and not affect our findings related to the relative Ω differences between isotopomers. The importance of polarization effects regarding the Ω differences of isomers or other closely related ions will be a subject of future research. Note in all cases that N2 is modeled as a sphere and its rotational changes are not considered. This is done to simplify the present calculations and isolate the effect of ion rotation. Additional effort can be directed toward integrating Ω dependence on the rotational properties of both colliding partners.

The energy transfer to an ion's rotational degrees of freedom is accounted for by evaluating the torque applied to the ion by N_2 as is shown in eq 7

$$\vec{\tau} = \sum_{i}^{N} \vec{r}_{\text{com},i} \times \vec{F}_{i} \tag{7}$$

where $\vec{r}_{\text{com, }i}$ is the distance of atom (i) from the CoM and \vec{F}_i is the LJ potential evaluated at atom (i). The total force (\vec{F}_{CoM}) exerted on the ion at a given time step is evaluated using eq 8:

$$\vec{F}_{\text{CoM}} = \sum_{i}^{N} \vec{F}_{i} \tag{8}$$

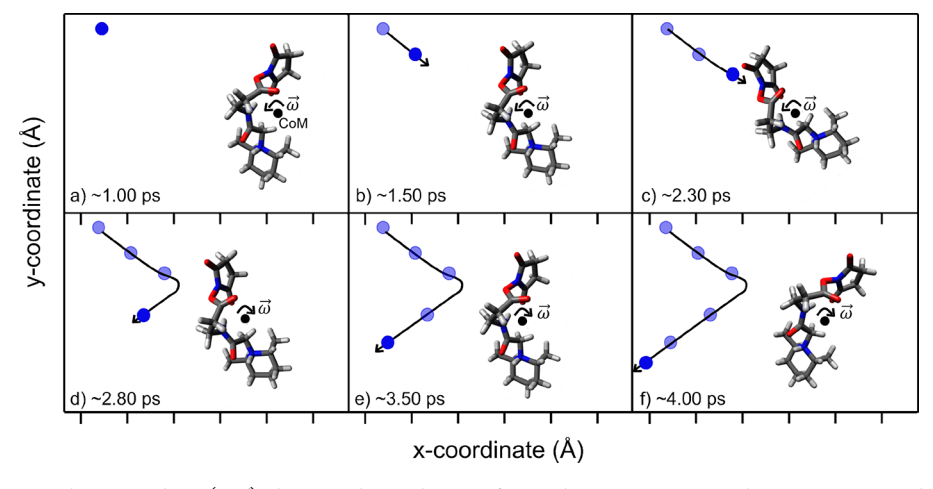


Figure 2. 2D illustration in the X-Y plane (a-f) showing the evolution of a single trajectory using the most accurate thermal ion rotation and translational to rotational energy $(TR-\varepsilon)$ model used in this work, and that accounts for pre- and post-collision effects. The blue sphere represents the position of N_2 at each time point, dark blue spheres represent the current position, while the lighter spheres represent the positions from previous time points.

Table 2. Simplified Overview of Computational Steps Taken during the Course of a Trajectory for the TR- ε , sTR- ε , rT- ε and T- ε Models Used in this Work

	TR- ε	sTR- ϵ	rT-ε	Τ-ε
	1 K-č			1-8
initialize starting conditions	$ec{v}_{ar{g}as}$, $ec{v}_{ar{ion}}$, $ec{\omega}_{ar{g}as}$	$\vec{v}_{\overline{g}as}$, $\vec{v}_{\overline{i}on}$, $\vec{\omega}_{\overline{g}as} = 0$	$ec{v}_{ m gas}$, $ec{v}_{ m ion}$, $ec{\omega}_{ m gas}$	$ec{v}_{\overline{ ext{gas}}}$ and $ec{v}_{\overline{ ext{ion}}}$ no description of $ec{\omega}_{\overline{ ext{vas}}}$
perform trajectory/evaluate forces	adjust:	adjust:	adjust:	adjust:
	$ec{v}_{\overline{\mathrm{g}}\mathrm{as}},\ ec{v}_{\overline{\mathrm{ion}}},\ ec{\omega}_{\overline{\mathrm{g}}\mathrm{as}}$	$ec{v}_{\overline{\mathrm{gas}}}$, $ec{v}_{\overline{\mathrm{ion}}}$, $ec{\omega}_{\overline{\mathrm{gas}}}$	$ec{v}_{\overline{ ext{gas}}}$ and $ec{v}_{\overline{ ext{ion}}}$	$ec{v}_{\overline{ ext{gas}}}$ and $ec{v}_{\overline{ ext{ion}}}$
	based on $\Phi(r)$ + τ	based on $\Phi(r)$ + τ	based on $\Phi(r)$	based on $\Phi(r)$
end simulation and calculate χ	evaluate:	evaluate:	evaluate:	evaluate:
	$ec{v}_{ ext{gas}}^{\scriptscriptstyle +}, ec{v}_{ ext{ion}}^{\scriptscriptstyle +}, ec{\omega}_{ ext{gas}}^{\scriptscriptstyle +}$	$\vec{v}_{\mathrm{gas}}^{\scriptscriptstyle +}, \vec{v}_{\mathrm{ion}}^{\scriptscriptstyle +}, \vec{\omega}_{\mathrm{gas}}^{\scriptscriptstyle +}$	$ec{v}_{ m gas}^{\scriptscriptstyle +}$ and $ec{v}_{ m ion}^{\scriptscriptstyle +}$	$ec{v}_{ m gas}^{\scriptscriptstyle +}$ and $ec{v}_{ m ion}^{\scriptscriptstyle +}$
Ω dependence on collision frequency	yes	no	yes	no
Ω dependence on translational to rotational energy transfer	yes	yes	no	no

which sums over force exerted across atoms. Through the inclusion/exclusion of eq 7, we can explore the differences due to energy transfer to the ion's rotational modes.

2.4. Collision Models. To understand the contribution of ion rotation to Ω and how best to model the contribution, we use four collision models to explore the relative importance of collisional frequency and energy transfer between translational and rotational modes as well as for comparison with experimental observations. All Ω calculations are performed using a temperature of 300 K. While a degree of ion heating may exist in TW-IMS experiments depending on the conditions employed, we anticipate that heating effects will affect the isotopomers nearly equally as their geometries are identical. Field heating effects are also anticipated to be negligible as the separations are not dependent on the TW conditions used. ²⁴

The first model includes ion thermal rotation ($T_{\rm r}=300~{\rm K}$) as well as the energy transfer to the ion's rotational modes during a collision via the evaluation of eq 7 during the dynamics. This is referred to as the thermal ion rotation and translational to rotational energy (${\rm TR-}\varepsilon$) model. This provides the most realistic model of the collision event compared to the other models and presumably is most reflective of experiment. In this model, the ion freely rotates about its CoM during the trajectory (Figure 2 provides a simple illustration of several times for a single trajectory of a TMT isotopomer ion). In Figure 2a,b, the ${\rm N}_2$ molecule and ion approach one another with the rotational motion of the ion in the counterclockwise

direction. Figure 2c shows the time at which the largest exchange of energy between the colliding partners occurs and N₂ is repelled from the ion. For subsequent time points (Figure 2d-f), both the N₂ molecule and the ion follow new trajectories with different velocities. In this case, there is a change in the ion's rotational motion (clockwise postcollision). The partitioning of energy from N2 to the translational and rotational motions of the ion can be evaluated by comparing the kinetic energy of N2 as well as the translational and rotational energies of the ion before and after a collision. A rotating molecule will have an increased collision frequency compared to a non-rotating molecule (and thus Ω to some extent) due to the 'blurring' effect described by Shvartsburg et al.³² Importantly, this first model captures the blurring effect of rotating ion and the corresponding change in collisional frequency as well as differences in translational to rotational energy transfer.

To study the effects of only the translational to rotational energy transfer (in the absence of collision frequency differences), we employ a second model, the simplified thermal ion rotation translational to rotational energy transfer collision model or sTR- ε model, which neglects the initial ion rotation ($\omega=0$, at the beginning of the trajectory as the ion and N₂ approach). The torque exerted on the ion by N₂ is still evaluated such that after a collision, the ion rotates in response to the torque applied by N₂ (i.e., has a non-zero post-collision rotational velocity) and the exchange of translational and rotational energy is accounted for. Since the rotational

Table 3. Average Ω Values for TMT-126 and TMT-127 Evaluated on a Non-relative and Relative Scale Using the TR- ε Model.

isotopomer	Ω (Å 2) run 1	Ω (Å 2) run 2	Ω (Ų) run 3	mean (Ų)
TMT-126	161.0774	161.1383	161.0650	161.0936 ± 0.0226
TMT-127	161.0944	161.1499	161.0862	161.1102 ± 0.0200
$\Delta\Omega_{127-126}$	0.0170	0.0117	0.0212	0.0166 ± 0.0028
isotopomer	adjusted Ω (Å 2) run 1	adjusted Ω (Å 2) run 1	adjusted Ω (Å 2) run 1	adjusted mean Ω (Å 2)
TMT-126 (ref)	161.0936	161.0936	161.0936	161.0936 ± 0.0000
TMT-127	161.1106	161.1053	161.1148	161.1102 ± 0.0028

temperature of the ion is initially 0 K, any differences in collision frequency due to rotation (and blurring) are ignored with this model while still accounting for translational to rotational energy transfer.

The third model employed is the static translational only energy transfer $(T-\varepsilon)$ model, which is akin to that used by the MobCal package and similar to other approaches for calculating Ω . ^{39,40} With this model, there is no evaluation of torque, eq 7, and the dynamics are performed with $\omega = 0$, which assumes no thermal rotation at the start of a trajectory and no evaluation of energy transfer to ion rotational modes during the collision. With this model, the ion retains its initial orientation for the duration of the trajectory. This model effectively serves as a control for parsing the effects of energy transfer and collision frequency. Finally, the rotating-T- ε (rT- ε) model uses a non-zero initial ion rotation to account for the 'blurring' effect on collision frequency, $T_r = 300 \text{ K}$, but ignores partitioning of energy to rotational modes (i.e., it assumes perfectly elastic collisions) by ignoring the contributions of torque, Eq. 7.

Table 2 summarizes the four models and the steps for computational implementation (taken at the start, during, and after each collision) for each. At the start of each trajectory (first row) the initial translational velocities of the ion $(v_{\rm ion}^-)$ and buffer gas $(v_{\rm gas}^-)$ are assigned based on a 20-pt Gaussian-Laguerre quadrature (see Figure S2) for all models, while assuming that the velocity of the ion is small enough to be negligible compared to that of the gas. For the TR- ε and rT- ε models, the initial rotational velocity of the ion $(\omega_{\rm ion}^-)$ is assigned using a gaussian random number generator based on a 300 K Boltzmann distribution of rotational velocities. For the sTR- ε model, $\omega_{\rm ion}^-$ is set to 0. No rotational motion is considered with the T- ε model, which is equivalent to assuming an infinite MoI for all ions.

After the initial velocities are assigned, a trajectory is started, and the velocities of both bodies are adjusted based on the force between the pair at each time step (second row of Table 2) and tracked using a leap-frog integrator.⁴¹ The force evaluated at each time-step for the TR- ε and sTR- ε models includes the contribution of torque, while the force in the T-arepsilonand rT- ε models is simply the sum of the LJ interaction potentials. The computation is repeated until the set trajectory time limit expires or N2 is >20 Å from the ion. The postcollision translational velocities of the ion and N_2 (v_{ion}^+ and $v_{\rm gas}^{+}$) are evaluated at a point where there is no longer an interaction between the colliding pair. The post-collision rotational velocity is computed for the TR- ε and sTR- ε models, $\omega_{\mathrm{ion}}^{+}$. The deflection angle after a collision is, in all cases, based on the post-collision velocity of N₂ $(v_{\rm gas}^{+})$ relative to before the collision (v_{gas}^{-}) (row 3 of Table 2). Once a trajectory is ended, a new trajectory is initialized with a different initial ion orientation, ω_{ion} , v_{ion} , and impact parameter, which is sampled quadratically in the range of 0

to $b_{\rm max}$ (the maximum impact parameter). The value for $b_{\rm max}$ is defined as the distance where $1-\cos(\chi)$ (χ being the deflection angle of the gas molecule pre- and post-collision) is less than 0.0005 radians, indicating negligible interaction between the gas and the molecule. The final Ω value is evaluated using eq 5. It is important to note that $v_{\rm gas}^+$ is sensitive to the magnitude of energy transfer during the trajectory, allowing the final deflection angle (χ) to act as a reporter for energy transfer, even though the assumption in eq 5 is that the collisions are elastic. Thus, calculation of Ω from the χ value using different models described above allows us to explore the two rotational contributions (i.e., collisional frequency and energy partitioning).

3. RESULTS AND DISCUSSION

The drift tube Ω measured values for TMT-126 and iodoTMT-126 are 180 \pm 1 and 189 \pm 1 A², which is typical of the best experimental measurements where their accuracy is no better than 0.5 to 1%. The Ω values for the global minimum structures used in this study are calculated to be 179.5 \pm 0.6 and 192.4 \pm 1.0 A² using the T- ε model while including the polarization term in eq 6. The agreement between the experimental and calculated values indicates that the global minimum structures used throughout this study are similar in Ω to the measured values. The remaining Ω calculations below exclude the polarization term from eq 6 for all models for the sake of computational speed, which should not otherwise impact this comparison. Removing this term results in a decrease in the calculated CCS as long-range interactions are ignored. As can be seen in Table S3, the calculated CCS for TMT-126 using the T- ε model while excluding the polarization term from eq 6 is \sim 167 A2, indicating the magnitude of this term for this ion. As noted above, the absolute Ω values calculated below for all models will be smaller than expected as they all are performed without the polarization term in the description of the potential. The focus of this work is to explore the rotational dependence of Ω through the different collision models, rather than exploring the accuracy of the calculated Ω value. Again, as we are dealing with isotopomers that have identical structures, the exclusion of the polarization should not affect the relative differences in Ω between isotopomers for any of the collision models.

 Ω values for each isotopomer are calculated for each model using 3 independent runs (N=3) (Figure S3). Each run represents an average of 24 independent trials that each employ $4\times 10^{+6}$ trajectories at each of the eight relative speeds sampled. These 72 independent trials ($\sim 2.3\times 10^{+9}$ trajectories for each isotopomer) use different "seeds", encompassing different rotational velocities, starting orientations, and impact parameters. The initial linear velocities are pre-defined with the quadrature and are identical for all trials (Figure S2). The incorporation of thermal rotation and energy transfer to rotational motion will influence the absolute value of Ω for a

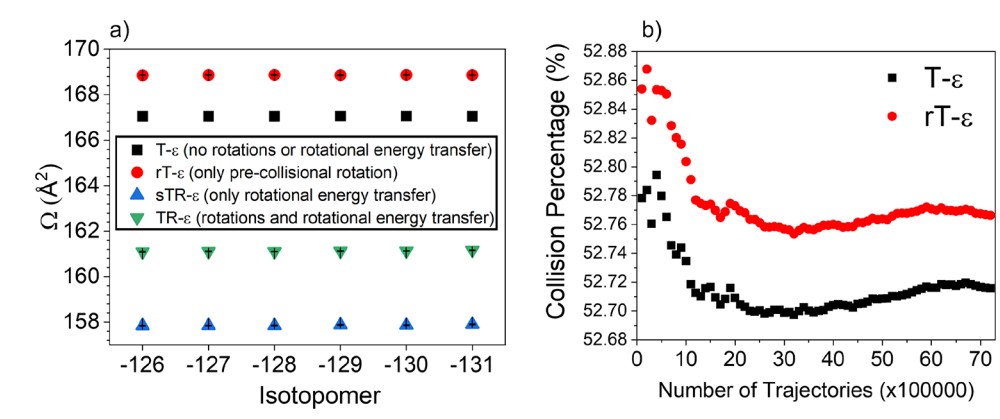
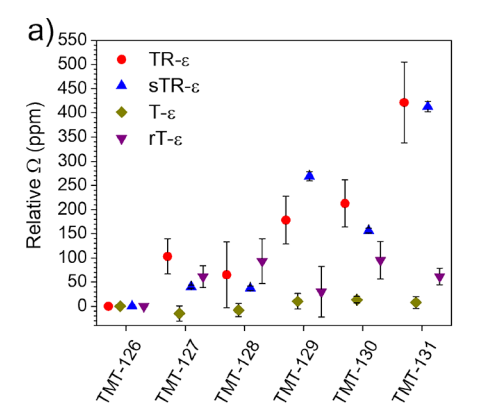


Figure 3. (a) Plot of Ω for the six TMT isotopomer ions computed using the four models showing the impact of including both thermal rotation (leading to differences in collision frequency) and energy transfer between translational and rotational degrees of freedom (TR- ε), only including thermal rotation (rT- ε), only including energy transfer to rotational motion (sTR- ε), and ignoring both properties (T- ε). (b) Plot of the percentage of collisions experienced by TMT-126 isotopomer as a function of the total number of trajectories for the T- ε and rT- ε models, showing an increase in the collision frequency for the rotating ion.

given isotopomer between models and the precision of the predictions, e.g., the $\Delta\Omega$ between isotopomers for a given model. In all cases, the average Ω across the 3 trials for the highest mobility isotopomer is set as the reference value to which the remaining isotopomers within that model and isotopomer set are referenced; the values of isotopomer -126in Table S3 represent these reference values for each model. Differences in the absolute Ω value for a given isotopomer between models is much larger than the difference between isotopomers in a given model as will be discussed below. To obtain the Ω values for the remaining isotopomers within a model, we calculate the average difference between the reference Ω and each of the remaining isotopomers for each run as is demonstrated in detail in Figure S3. An example of this is provided in Table 3, where the Ω values are provided for TMT isotopomer -126 and -127 evaluated using the TR- ε model. The first two rows list the mean values evaluated for each run as well as the mean and the standard error of the mean across the 3 runs. The third row lists the difference between the two isotopomers for each run - recall that within a run, isotopomers are sampled over identical conditions; between runs, the sampled conditions differ slightly due to the use of different "seed" values. The mean difference here represents the relative increase in Ω of -127 relative to -126along with the standard error of the mean difference for the isotopomers across runs. The last two rows show the Ω values obtained when shifting each run to a common reference. This is done by setting the mean value of TMT-126 across the 3 runs as the common reference value. The adjusted Ω values for TMT-127 are then evaluated by adding the difference between TMT-127 and TMT-126, for each run, to the common reference value. In this manner, Ω differences due to slightly different sampling conditions between runs are normalized such that differences in Ω are only due to the differences in collision frequency and translational to rotational energy transfer. The new average Ω value and its standard error associated with TMT-127 represents the magnitude of the increase in Ω relative to -126 as well as its uncertainty. This process is repeated for all isotopomers within a given model. In this manner, we are able to isolate the differences between isotopomers and the precision with which Ω can be predicted (i.e., the $\Delta\Omega$ of -126 (reference) and -1xx). The associated error for the calculated Ω values is represented using the

standard error (SE), $\sigma/\operatorname{sqrt}(N)$, of the mean Ω or mean $\Delta\Omega$ (when plotted on a relative scale). The SE is chosen as each trial (N) samples over different orientations and rotational speeds (TR- ε and rT- ε models), where the SE represents how far the mean of a given trial differs from the mean across all trials.

Figure 3a plots the Ω values for all TMT isotopomers predicted using the four models and reveals that each model yields a somewhat different value of Ω for the TMT isotopomers. The Ω values for all four models are provided in Table S3 along with the values for the iodoTMT isotopomers. At this level of analysis, all isotopomers behave similarly as small differences in Ω between isotopomers because their slightly different CoM and MoI (effecting collision frequency and energy transfer between modes) are much smaller ($\sim 0.06 \text{ Å}^2$) compared to the $\sim 2-3 \text{ Å}^2$ difference between models. The difference in Ω for a given isotopomer between models is of interest as it provides insight on the consequence of ignoring ion rotation and the inelasticity of collisions on the Ω prediction accuracy. For example, in comparing the two models that do not account for energy transfer to rotational motion (T- ε and rT- ε), we see an $\sim 2 \text{ Å}^2$ difference in the predicted Ω for all isotopomers. The simplest T- ε model (and by far the most broadly used with IMS for Ω computation) only considers translational modes of the collision partners, while the rT- ε model allows for the thermal rotation of the ion. The increase in Ω predicted with the rT- ε model is a consequence of the increased collision frequency due to the blurring effect. This can be explicitly observed in Figure 3b, where the collision percentage (# of collisions/# of trajectories \times 100) for the T- ε and rT- ε model is plotted as a function of the first $7.2 \times 10^{+6}$ trajectories. By modeling the thermal rotation of the ion, we see that the number of collisions experienced is about 0.06% higher compared to its non-rotating counterpart, leading to the observed increase of 2 A^2 in Ω between models. A similar increase in Ω can be observed when comparing the two models, which do account for energy transfer to rotational degrees of freedom (sTR- ε and $TR-\varepsilon$) in Figure 3a. The $TR-\varepsilon$ model, which does allow for ion thermal rotation, yields Ω values that are increased by 3 Å² compared to the sTR- ε model, which ignores ion thermal rotation. Thus, in both cases for the TMT structure, when thermal rotation is added, there is a corresponding increase in



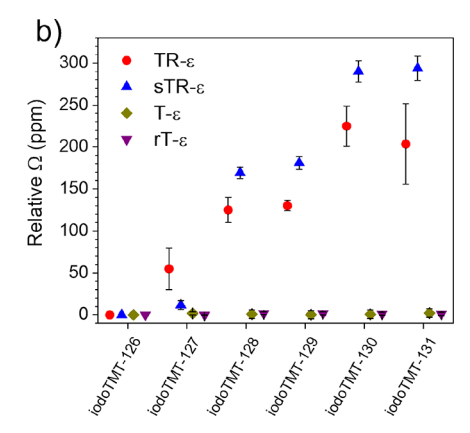


Figure 4. Relative change in Ω between TMT (a) and iodoTMT (b) isotopomers in terms of ppm as calculated by the four models.

the predicted Ω . For iodoTMT, this effect is less pronounced where the T- ε and rT- ε converge to nearly the same values, see Table S3. The less pronounced effect of collision frequency on Ω for iodoTMT is related to its more spherical geometry compared to the TMT geometry (Figure S1), which is consistent with what would be expected from the work of Shvartsburg et al.

Note that there is a further difference in Ω caused by the incorporation of energy transfer to rotational motion. For example, the TR- ε and rT- ε models both account for thermal rotation. However, the rT- ε model ignores energy transfer to rotational motion while the TR- ε does not. As a result, the Ω values predicted using the TR- ε model are ~8 A² smaller than those predicted using the rT- ε model for TMT. A similar trend is observed for iodoTMT where the difference in the Ω value for the rT- ε model is ~5 Å² larger than what is predicted using the TR- ε model. This arises from the collisional energy relaxing into the rotational modes and a corresponding decrease in the collisional energy damping the translational motion of the ion. This is again seen in comparing the T- ε and sTR-arepsilon models, both of which ignore thermal rotation but the sTR- ε model accounts for energy transfer to rotational motion. The Ω values predicted with sTR- ε model are ~9 and ~ 6 Å² smaller than those predicted with the T- ε model for TMT and iodoTMT, respectively. In both cases, there is a corresponding reduction in the predicted Ω value when energy transfer to rotational motion is considered. Interestingly, the effect of translational to rotational energy exchange has a more pronounced effect on the value of Ω compared to the effect of collision frequency (compare difference in Ω between sTR- ε and $T-\varepsilon$ vs $T-\varepsilon$ and $rT-\varepsilon$). When the energy transfer to rotational motion is ignored, it effectively models the MoI of the ion as infinite and assumes no partitioning of energy to the ion's rotational motion, e.g., there is no coupling of translational to rotational energy. In reality, it appears that the MoI of ions of this molecular weight (~ 500 amu, and size \sim 160–180 A²) is low enough where there can be sizable contributions to Ω via energy transfer to rotational motion.

Overall, the general trends in the predicted Ω values between the four model is consistent with our expectations. The rT- ε model tends to yield larger values of Ω , as it accounts for the increased collision frequency of a rotating ion but assumes that there is no energy transfer to the rotation motion upon a collision; while the sTR- ε model predicts the smallest values of Ω as it assumes a non-rotating ion while accounting for energy transfer to rotational motion during a collision

event. Between models, the Ω value for a given isotopomer changes depending on the description of the collision process. While the focus of this work is not on the accuracy of the calculated Ω values, the data provided in Figure 3a is of interest regarding the use of LJ potentials. LJ potentials for collisions with N2 are obtained by adjusting previously determined σ and ε values to minimize the error between calculated Ω values, using collision models most similar to the T- ε model described in this text, and experimentally measured values for several compounds ranging in size and mass. 18 The comparison in Figure 3a shows that the calculated Ω will change if the collision dynamics account for the rotational properties of a given structure. As such, it can be expected that the LJ parameters would have to be reparametrized when using a collision model, which accounts for rotational properties such that the calculated Ω value would be consistent with measured Ω values for systems with well-defined geometries, e.g., C60. In this regard, the accuracy of Ω predictions should be further investigated and benchmarked to experimental measurements as currently most Ω calculations ignore both the thermal rotation and energy transfer to rotational modes.

The relative Ω shift between isotopomers predicted by the TR- ε (red), sTR- ε (blue), T- ε (gold), and rT- ε (purple) models are plotted in Figure 4a,c. The values plotted here are identical to those provided in Table S3; however, the Ω values are plotted on a relative scale in terms of a ppm shift relative to the -126 isotopomer $((\Omega_{1xx} - \Omega_{126})/\Omega_{126}) \times 1 \times 10^{+6}$, for ease of comparison. The most rigorous TR- ε model clearly shows significant differences in relative Ω shift between isotopomers; i.e., the $\Delta\Omega$ between -126 and -1xx for both the TMT and iodoTMT isotopomers. The average SE of the mean of these values across isotopomers is approx. $\pm 0.0047\%$ (approx. ± 47 ppm) and approx. $\pm 0.0024\%$ (approx. ± 24 ppm) for TMT and iodoTMT, respectively. The SE of the mean value decreases as the number of trajectories is increased (relationship of 1/sqrt(trajectories); however the value to which the mean converges has an accuracy limited by the description of the collision interaction. In contrast with the TR- ε model, the T- ε model is fundamentally limited by its description of collision process and cannot predict Ω differences between isotopomers. This is explicitly demonstrated in Figure 4a,c where there are no significant differences in Ω predicted with the T- ε model (gold diamonds) between isotopomers of TMT and iodoTMT. Note that the number of trajectories and the sampled conditions between the T- ε and TR- ε models are identical, indicating that the lack of resolution

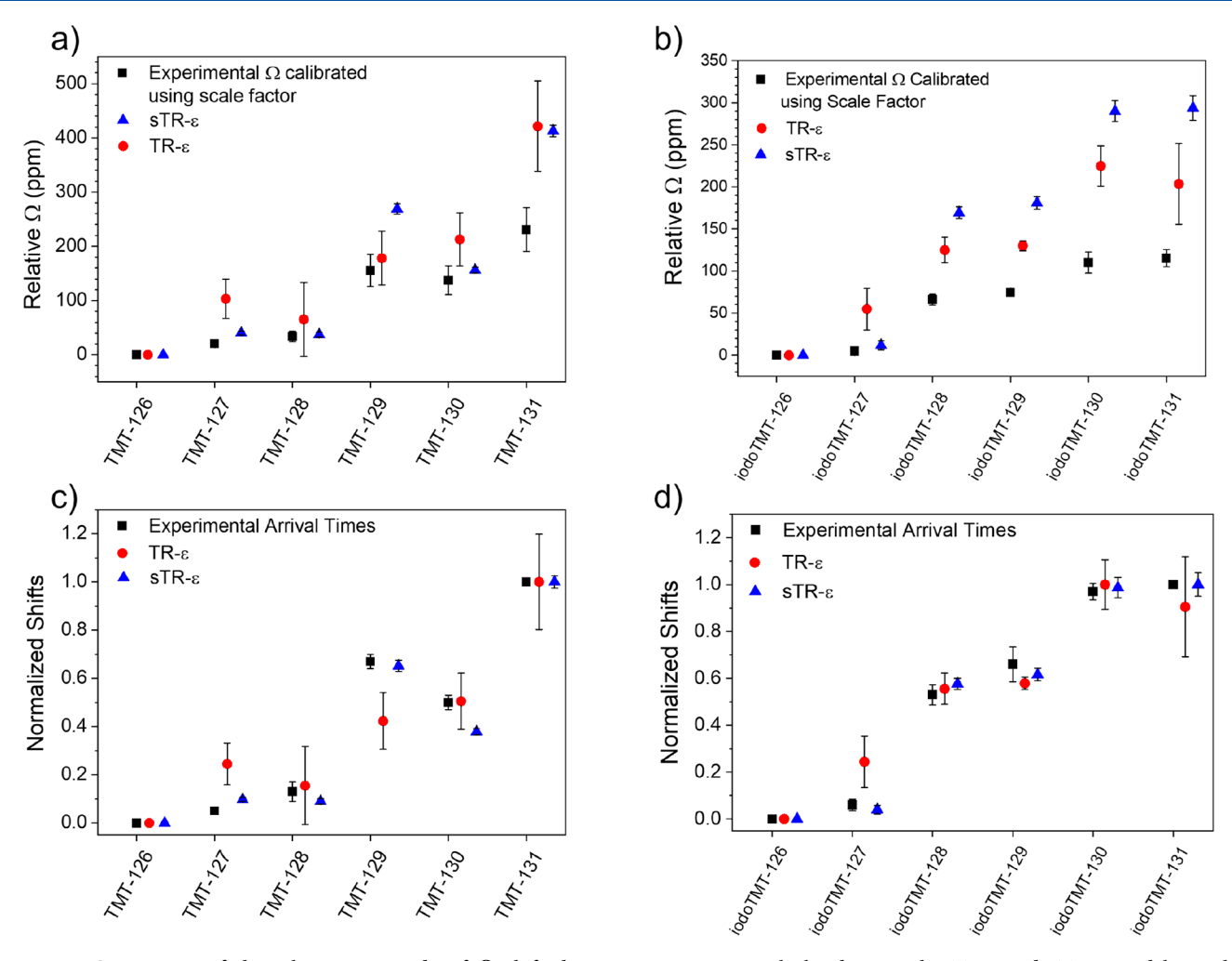


Figure 5. Comparison of the relative magnitude of Ω shifts between isotopomers calculated using the TR- ε and sTR- ε models to the experimentally estimated Ω shifts using the scale factor method discussed in the text for TMT (a) and iodoTMT (b). Comparison of the relative differences in arrival time and computed Ω values computed using the TR- ε and sTR- ε models on a normalized scale for TMT (c) and iodoTMT (d).

within the T- ε model is not due to an insufficient number of trajectories performed but rather an insufficient description of the collision process. Since the T- ε model only describes the exchange of linear momentum, it cannot account for Ω differences related to rotation, in contrast to the TR- ε model's more accurate description that allows the isotopomers to be distinguished.

The rT- ε model (purple) provides insight into the contribution of collision frequency or the 'blurring effect' on the relative Ω values between isotopomers. For both TMT and iodoTMT, there is virtually no difference in the relative Ω values when only collision frequency is considered, indicating that the blurring effect differences have less impact than differences in energy transfer between translational and rotational modes, for isotopomers. Larger changes in CoM and MoI, e.g., in the case of isomers, may result in a larger contribution of the blurring effect on Ω differences. The negligible contribution of collision frequency on Ω differences shown here however is consistent with the similar predictions between the TR- ε and sTR- ε models as the sTR- ε model assumes an identical number of collisions between isotopomers while accounting for differences in energy partitioning between isotopomers. The slight differences between these models (e.g., magnitude of the Ω shift of -1xx to the reference -126

isotopomer) is most likely related to how the collision energetics are modeled: in the sTR- ε , the relative translational speeds of the ion and N₂ gas is set using the quadrature and the rotational velocity of each isotopomer is set to zero precollision such that the starting kinetic energy of all isotopomers are identical. In the TR-arepsilon model, the differences in rotational velocities are accounted for pre-collision as each isotopomer has an assigned rotational velocity based on its MoI and thus slightly different kinetic energies. As a result, the energetics of each collision differs between isotopomers when the rotational velocity differences are explicitly accounted for, which may further influence the translational to rotational energy transfer between N₂ and a given isotopomer. These differences are ignored in the sTR- ε model. Overall, however, we find that the Ω differences between isotopomers are largely dependent on differences in energy transfer rather than collision frequency. Furthermore, the relative shifts between isotopomers agree fairly well between both models indicating that predictions can be made with the sTR- ε model, which is about 10× more efficient computationally.

The relative shift in Ω between the -126 and -131 isotopomers is estimated to be $\sim\!450$ ppm for TMT and between 200 and 280 ppm for iodoTMT depending on the model employed. The experimental Ω differences obtained via

calibration using the scale factor, as described above, are plotted with black squares in Figure 5a,b for TMT and iodoTMT and are compared to the calculated Ω differences obtained using TR- ε are sTR- ε models (values provided in Table S4). Overall, the comparison between the estimated and calculated Ω differences demonstrate a good level of agreement. Calibration using the scale factor is anticipated to result in an underestimation of the magnitude of the Ω differences between isotopomers. We do not however expect the actual Ω differences between isotopomers to differ significantly from this estimation due to the fact that the separation between -131 and its [M + 1] + isotopologue is of a similar magnitude $(0.5\times)$ to the maximum separation between isotopomers for a given set. Thus, we estimate that the Ω differences obtained via calibration using the scale factor are within a factor of about 2 to their actual values. Consistent with this, the calculated mobility differences (using the TRand sTR- ε models) are consistently larger than what is estimated using the scale factor but all fall within a factor of 2- $3\times$ from the estimated Ω differences from the scale factor.

For reference, the Ω differences between the -131 isotopomer and its [M + 1] + isotopologue were also calculated using the sTR- ε model (averaging over its four possible isotopomers, see Figure 1) such that calculated Ω differences can be compared to the Ω differences anticipated based on the change in reduced mass alone. The calculated differences between the -131 isotopomer and its [M + 1] +isotopologue are 169 and 143 ppm for TMT and iodoTMT, respectively. Compared to the calculated Ω differences of 108 and 66 ppm based on the reduced mass alone (values provided in Table S5), it appears that the $\Delta\Omega$ between the -131 isotopomer and its [M + 1] + isotopologue differs by about two-fold from when the rotational properties are considered. While additional experimental efforts are needed to better calibrate the CCS differences more accurately over this small mobility range, this initial calculation of the absolute Ω differences between isotopomers appears reasonable.

Alternatively, rather than gauging the relative magnitude of the Ω differences between isotopomers, one can compare how well the relative Ω differences can be predicted. As seen above, to compare the magnitude of the calculated differences, the mobility scale must be calibrated in an accurate manner, which at this time we can only provide an estimate of that scale. Thus, we provide an alternative comparison using the relative arrival times and the calculated Ω differences on a normalized scale. For this comparison, we assume the differences in arrival times to be linearly correlated to differences in Ω over the small mobility range. In this comparison, the arrival time shifts (Table S1) are normalized, as done previously, 23,24 by linearly shifting the arrival times of all isotopomers such that the arrival time of the highest mobility isotopomer is set to zero. The adjusted arrival times are then normalized to the adjusted arrival time of the lowest mobility isotopomer. A similar procedure is done for the calculated Ω values. A comparison of the experimental (black squares) and calculated normalized shifts, using the TR-arepsilon and sTR-arepsilon models, in Ω are plotted in Figure 5c,d for TMT and iodoTMT, and values are provided in Table S6. In performing this comparison, we are able to address how well the relative shifts in Ω between isotopomers -127 through -130 can be calculated with both computational models. In this comparison both models appear to effectively reproduce the relative changes in Ω between isotopomers. For the TMT isotopomer set (Figure 5c), the

sTR- ε model predicts the relative change in Ω with near perfect agreement, where the relative difference in Ω for TMT-130 is slightly under predicted. The TR- ε model shows a slightly worse agreement, where the relative Ω of TMT-127 is predicted to be slightly higher than the experimental relative difference in arrival time and the relative Ω value of TMT-129 is slightly under predicted. Overall, however the deviation is small and the overall trend between the relative computed Ω values agrees well with the relative differences in experimental arrival times. For the iodoTMT isotopomer set (Figure 5d), we see that within the error of the experimental relative differences, the computed relative differences in Ω are all in agreement for both collision models. Determining the magnitude of Ω differences is indeed important and will be useful for future high-resolution separation; however, in this current work we demonstrate that the relative differences in Ω can be accurately predicted (normalized scale) and the calculated magnitude of the differences, to our best estimation, may deviate by a factor of \sim 2.5 from their actual values.

4. CONCLUSIONS

Experimental Ω differences (estimated to be $\lesssim 50-450$ ppm) between isotopomers (same mass and 3-D structure; differing only in the distribution of mass) can be observed but cannot be accounted for using traditional approaches of calculating Ω . To account for the differences in Ω , we have developed an approach for high-precision Ω calculations that accounts for Ω 's dependence on the ion's rotational properties (MoI and CoM). In doing this, we explicitly account for the increases in collision frequency for an ion undergoing thermal rotation as well as the energy partitioning between translational and rotational degrees of freedom upon an ion-neutral collision. We find that by accounting for the thermal rotation of an ion, a corresponding increase in Ω may be observed depending on the ion geometry, which can be rationalized by an increase in the number of collisions the ion experiences. We find however that differences in collision frequency alone do not account for Ω differences between isotopomers, indicating that the change in collision frequency between the isotopomers of a given set is negligible. Our results further support that the main cause of Ω differences between isotopomers is related to the difference in the energy partitioning between translational and rotational degrees of freedom. Differences in the MoI between isotopomers influences the amount of energy exchanged during a collision between the ion and buffer gas, which directly impacts the momentum transfer cross section, which is dependent on the amount of momentum exchange between colliding partners per unit time.

Experimentally, it has been demonstrated that Ω differences of \lesssim 50 ppm are readily discernable (such small differences in Ω are driven by the difference in rotational properties as the 3D structures are identical), while computationally, a similar or better level of precision is obtainable. We find that the relative change in Ω (i.e., relative increase from one isotopomer to another) between isotopomers can be predicted accurately with a high level of precision when a low energy structure is used for the calculation of $\Delta\Omega$. The predictive capability demonstrated here will prove useful as the number of ultrahigh-resolution and, more specifically, ultrahigh-precision IMS measurements increases. The separations observed at lower resolutions are indeed driven by conformational differences between ion species. However, separations observed with path lengths of several hundreds of meters for

multipass separations need to be accounted for using more sophisticated collision dynamics as detailed in this work. Separations in which ions that begin to resolve after hundreds of meters of TW separation will be influenced by their differences in rotational properties. The ability to accurately predict these relative shifts and even their magnitude will prove useful for the identification of compounds that have highly similar mobilities. The predictive capabilities demonstrated here as well as the precision of the IMS measurements show promise for the coupling of ultrahigh-resolution ion mobility spectrometry and Ω predictions to distinguish between and identify structurally similar isomers and conformers based on their relative mobility differences. The ability to quickly, precisely, and accurately predict differences in Ω between sets of candidate structures may prove useful for high-confidence molecular annotation.

ASSOCIATED CONTENT

Solution Supporting Information

The Supporting Information is available free of charge at https://pubs.acs.org/doi/10.1021/acs.jpca.3c01264.

Figure of 3-D geometries of the TMT and iodoTMT structures employed in the simulations, table of experimental relative arrival times, table of Lennard-Jones potentials employed, figures of 20-pt Gaussian-Laguerre quadrature used for N_2 and ion relative speeds, computational method for obtaining relative Ω values and associated text, table of calculated Ω values for TMT and iodoTMT isotopomer for each collision model, table of relative MoI and estimated relative Ω values (using scale factor)/calculated mobility differences, table of relative arrival times of $[M+1]^+$ isotopologue of 131 to -131 along with relative MoI increases and calculated mobility differences using sTR- ε model, table of normalized arrival times and Ω shifts for TMT and iodoTMT isotopomers (PDF)

AUTHOR INFORMATION

Corresponding Author

Christopher P. Harrilal — Biological Sciences Division, Pacific Northwest National Laboratory, Richland, Washington 99354, United States; Occid.org/0000-0003-0576-1709; Email: christopher.harrilal@pnnl.gov

Authors

Sandilya V.B Garimella — Biological Sciences Division, Pacific Northwest National Laboratory, Richland, Washington 99354, United States; orcid.org/0000-0001-6649-9842

Jaehun Chun – Physical and Computational Sciences
Directorate, Pacific Northwest National Laboratory,
Richland, Washington 99354, United States; ○ orcid.org/
0000-0002-2291-6496

Nikhil Devanathan — Biological Sciences Division, Pacific Northwest National Laboratory, Richland, Washington 99354, United States

Xueyun Zheng — Biological Sciences Division, Pacific Northwest National Laboratory, Richland, Washington 99354, United States; Oorcid.org/0000-0001-9782-4521

Yehia M Ibrahim — Biological Sciences Division, Pacific Northwest National Laboratory, Richland, Washington 99354, United States; Oorcid.org/0000-0001-6085-193X Carlos Larriba-Andaluz — Department of Mechanical and Energy Engineering, IUPUI, Indianapolis, Indiana 46202, United States; orcid.org/0000-0003-0864-7733

Gregory Schenter – Physical and Computational Sciences Directorate, Pacific Northwest National Laboratory, Richland, Washington 99354, United States

Richard D. Smith — Biological Sciences Division, Pacific Northwest National Laboratory, Richland, Washington 99354, United States

Complete contact information is available at: https://pubs.acs.org/10.1021/acs.jpca.3c01264

Author Contributions

The manuscript was written through contributions of all authors. All authors have given approval to the final version of the manuscript.

Notes

The authors declare no competing financial interest.

ACKNOWLEDGMENTS

The efforts at PNNL were supported by the PNNL m/q Initiative- a Laboratory Directed Research and Development Program at PNNL. R.D.S. would like to acknowledge support by the National Institute of General Medical Sciences, P41 GM103493-15. C.L. would like to acknowledge support by the NSF Division of Chemistry under grant nos. 1904879 and 2203968. Measurements were performed in the Environmental Molecular Sciences Laboratory, a DOE OBER national scientific user facility at PNNL. PNNL is a multiprogram national laboratory operated by Battelle for the DOE under contract DE-AC05-76RL01830.

■ REFERENCES

- (1) Dodds, J. N.; May, J. C.; McLean, J. A. Correlating Resolving Power, Resolution, and Collision Cross Section: Unifying Cross-Platform Assessment of Separation Efficiency in Ion Mobility Spectrometry. *Anal. Chem.* **2017**, *89*, 12176–12184.
- (2) Kanu, A. B.; Dwivedi, P.; Tam, M.; Matz, L.; Hill, H. H., Jr. Ion Mobility-Mass Spectrometry. J. Mass Spectrom. 2008, 43, 1–22.
- (3) Maurer, M. M.; Donohoe, G. C.; Valentine, S. J. Advances in Ion Mobility-Mass Spectrometry Instrumentation and Techniques for Characterizing Structural Heterogeneity. *Analyst* **2015**, *140*, *6782*–6798
- (4) Cumeras, R.; Figueras, E.; Davis, C. E.; Baumbach, J. I.; Gràcia, I. Review on Ion Mobility Spectrometry. Part 1: Current Instrumentation. *Analyst* **2015**, *140*, 1376–1390.
- (5) Zhao, B.; Bian, X.; Zhuang, X.; Liu, S.; Liu, Z.; Song, F. Screening apo-SOD1 Conformation Stabilizers from Natural Flavanones Using Native Ion Mobility Mass Spectrometry and Fluorescence Spectroscopy Methods. *Rapid Commun. Mass Spectrom.* 2022, 36, No. e9251.
- (6) Rolland, A. D.; Biberic, L. S.; Prell, J. S. Investigation of Charge-State-Dependent Compaction of Protein Ions with Native Ion Mobility—Mass Spectrometry and Theory. J. Am. Soc. Mass Spectrom. 2022, 33, 369–381.
- (7) Turzo, S. M. B. A.; Seffernick, J. T.; Rolland, A. D.; Donor, M. T.; Heinze, S.; Prell, J. S.; Wysocki, V. H.; Lindert, S. Protein Shape Sampled by Ion Mobility Mass Spectrometry Consistently Improves Protein Structure Prediction. *Nat. Commun.* **2022**, *13*, 4377.
- (8) Uetrecht, C.; Rose, R. J.; van Duijn, E.; Lorenzen, K.; Heck, A. J. R. Ion Mobility Mass Spectrometry of Proteins and Protein Assemblies. *Chem. Soc. Rev.* **2010**, *39*, 1633–1655.
- (9) Eldrid, C.; Ujma, J.; Kalfas, S.; Tomczyk, N.; Giles, K.; Morris, M.; Thalassinos, K. Gas Phase Stability of Protein Ions in a Cyclic Ion

- Mobility Spectrometry Traveling Wave Device. *Anal. Chem.* **2019**, *91*, 7554–7561.
- (10) Jin, C.; Harvey, D. J.; Struwe, W. B.; Karlsson, N. G. Separation of Isomeric O-Glycans by Ion Mobility and Liquid Chromatography-Mass Spectrometry. *Anal. Chem.* **2019**, *91*, 10604–10613.
- (11) Wu, Q.; Wang, J.-Y.; Han, D.-Q.; Yao, Z.-P. Recent Advances in Differentiation of Isomers by Ion Mobility Mass Spectrometry. *TrAC*, *Trends Anal. Chem.* **2020**, *124*, No. 115801.
- (12) Wu, F.; Wu, X.; Chi, C.; Ding, C.-F. Simultaneous Differentiation of C= C Position Isomerism in Fatty Acids through Ion Mobility and Theoretical Calculations. *Anal. Chem.* **2022**, *94*, 12213–12220.
- (13) Burnum-Johnson, K. E.; Zheng, X.; Dodds, J. N.; Ash, J.; Fourches, D.; Nicora, C. D.; Wendler, J. P.; Metz, T. O.; Waters, K. M.; Jansson, J. K.; Smith, R. D.; Baker, E. S. Ion mobility Spectrometry and the Omics: Distinguishing Isomers, Molecular Classes and Contaminant Ions in Complex Samples. *TrAC, Trends Anal. Chem.* **2019**, *116*, 292–299.
- (14) Zhang, X.; Quinn, K.; Cruickshank-Quinn, C.; Reisdorph, R.; Reisdorph, N. The Application of Ion Mobility Mass Spectrometry to Metabolomics. *Curr. Opin. Chem. Biol.* **2018**, *42*, 60–66.
- (15) Fenn, L. S.; Kliman, M.; Mahsut, A.; Zhao, S. R.; McLean, J. A. Characterizing ion Mobility-Mass Spectrometry Conformation Space for the Analysis of Complex Biological Samples. *Anal. Bioanal. Chem.* **2009**, 394, 235–244.
- (16) Gabelica, V.; Marklund, E. Fundamentals of Ion Mobility Spectrometry. *Curr. Opin. Chem. Biol.* **2018**, 42, 51–59.
- (17) Revercomb, H. E.; Mason, E. A. Theory of Plasma Chromatography/Gaseous Electrophoresis. Review. *Anal. Chem.* **1975**, *47*, 970–983.
- (18) Campuzano, I.; Bush, M. F.; Robinson, C. V.; Beaumont, C.; Richardson, K.; Kim, H.; Kim, H. I. Structural Characterization of Drug-like Compounds by Ion Mobility Mass Spectrometry: Comparison of Theoretical and Experimentally Derived Nitrogen Collision Cross Sections. *Anal. Chem.* **2012**, *84*, 1026–1033.
- (19) Kalapothakis, J. M. D.; Barran, P. E. *Ion Mobility Mass Spectrometry Principles*; Springer Berlin Heidelberg: Berlin, Heidelberg, 2013; pp. 1142—1148.
- (20) Shvartsburg, A. A.; Smith, R. D. Fundamentals of Traveling Wave Ion Mobility Spectrometry. *Anal. Chem.* **2008**, *80*, 9689–9699.
- (21) Deng, L.; Webb, I. K.; Garimella, S. V.; Hamid, A. M.; Zheng, X.; Norheim, R. V.; Prost, S. A.; Anderson, G. A.; Sandoval, J. A.; Baker, E. S.; Ibrahim, Y. M.; Smith, R. D. Serpentine Ultralong Path with Extended Routing (SUPER) High Resolution Traveling Wave Ion Mobility-MS Using Structures for Lossless Ion Manipulations. *Anal. Chem.* **2017**, *89*, 4628–4634.
- (22) Webb, I. K.; Garimella, S. V.; Tolmachev, A. V.; Chen, T.-C.; Zhang, X.; Norheim, R. V.; Prost, S. A.; LaMarche, B.; Anderson, G. A.; Ibrahim, Y. M.; Smith, R. D. Experimental Evaluation and Optimization of Structures for Lossless Ion Manipulations for Ion Mobility Spectrometry with Time-of-Flight Mass Spectrometry. *Anal. Chem.* **2014**, *86*, 9169–9176.
- (23) Wojcik, R.; Nagy, G.; Attah, I. K.; Webb, I. K.; Garimella, S. V.; Weitz, K. K.; Hollerbach, A.; Monroe, M. E.; Ligare, M. R.; Nielson, F. F.; Norheim, R. V.; Renslow, R. S.; Metz, T. O.; Ibrahim, Y. M.; Smith, R. D. SLIM Ultrahigh Resolution Ion Mobility Spectrometry Separations of Isotopologues and Isotopomers Reveal Mobility Shifts due to Mass Distribution Changes. *Anal. Chem.* **2019**, *91*, 11952–11962.
- (24) Harrilal, C. P.; Gandhi, V. D.; Nagy, G.; Chen, X.; Buchanan, M. G.; Wojcik, R.; Conant, C. R.; Donor, M. T.; Ibrahim, Y. M.; Garimella, S. V. B.; et al. Measurement and Theory of Gas-Phase Ion Mobility Shifts Resulting from Isotopomer Mass Distribution Changes. *Anal. Chem.* **2021**, 14966.
- (25) Williamson, D. L.; Nagy, G. Isomer and Conformer-Specific Mass Distribution-Based Isotopic Shifts in High-Resolution Cyclic Ion Mobility Separations. *Anal. Chem.* **2022**, *94*, 12890–12898.

- (26) Larriba-Andaluz, C. A Perspective on the Theoretical and Numerical Aspects of Ion Mobility Spectrometry. *Int. J. Mass Spectrom.* **2021**, 470, No. 116719.
- (27) Zanotto, L.; Heerdt, G.; Souza, P. C. T.; Araujo, G.; Skaf, M. S. High performance Collision Cross Section Calculation-HPCCS. *J. Comput. Chem.* **2018**, *39*, 1675–1681.
- (28) Larriba-Andaluz, C.; Prell, J. S. Fundamentals of Ion Mobility in the Free Molecular Regime. Interlacing the Past, Present and Future of Ion Mobility Calculations. *Int. Rev. Phys. Chem.* **2020**, *39*, 569–623. (29) Alexeev, Y.; Fedorov, D. G.; Shvartsburg, A. A. Effective Ion Mobility Calculations for Macromolecules by Scattering on Electron Clouds. *J. Phys. Chem. A* **2014**, *118*, 6763–6772.
- (30) Larriba, C.; Hogan, C. J., Jr. Free Molecular Collision Cross Section Calculation Methods for Nanoparticles and Complex Ions with Energy Accommodation. *J. Comput. Phys.* **2013**, *251*, 344–363.
- (31) Gandhi, V. D.; Short, K.; Hua, L.; Rodríguez, I.; Larriba-Andaluz, C. A Numerical Tool to Calculate Ion Mobility at Arbitrary Fields From All-Atom Models. *J. Aerosol Sci.* **2023**, *169*, No. 106122.
- (32) Shvartsburg, A. A.; Mashkevich, S. V.; Siu, K. W. M. Incorporation of Thermal Rotation of Drifting Ions into Mobility Calculations: Drastic Effect for Heavier Buffer Gases. *J. Phys. Chem. A* **2000**, *104*, 9448–9453.
- (33) Stow, S. M.; Causon, T. J.; Zheng, X.; Kurulugama, R. T.; Mairinger, T.; May, J. C.; Rennie, E. E.; Baker, E. S.; Smith, R. D.; McLean, J. A.; et al. An Interlaboratory Evaluation of Drift Tube Ion Mobility—Mass Spectrometry Collision Cross Section Measurements. *Anal. Chem.* **2017**, *89*, 9048—9055.
- (34) Mohamadi, F.; Richards, N. G. J.; Guida, W. C.; Liskamp, R.; Lipton, M.; Caufield, C.; Chang, G.; Hendrickson, T.; Still, W. C. Macromodel—An Integrated Software System for Modeling Organic and Bioorganic Molecules Using Molecular Mechanics. *J. Comput. Chem.* 1990, 11, 440–467.
- (35) Lee, C.; Yang, W.; Parr, R. G. Development of the Colle-Salvetti Correlation-Energy Formula into a Functional of the Electron Density. *Phys. Rev. B* **1988**, *37*, 785.
- (36) Becke, A. D. Density-Functional Thermochemistry. I. The effect of the Exchange-Only Gradient Correction. *J. Chem. Phys.* **1992**, 96, 2155–2160.
- (37) Grimme, S.; Ehrlich, S.; Goerigk, L. Effect of the Damping Function in Dispersion Corrected Density Functional Theory. *J. Comput. Chem.* **2011**, 32, 1456–1465.
- (38) Frisch, M. J.; Trucks, G. W.; Schlegel, H. B.; Scuseria, G. E.; Robb, M. A.; Cheeseman, J. R.; Scalmani, G.; Barone, V.; Petersson, G. A.; Nakatsuji, H. et al. *Gaussian 16 Rev. C.01*; Gaussian Inc.: Wallingford, CT, 2016.
- (39) Mesleh, M. F.; Hunter, J. M.; Shvartsburg, A. A.; Schatz, G. C.; Jarrold, M. F. Structural Information from Ion Mobility Measurements: Effects of the Long-Range Potential. *J. Phys. Chem.* **1996**, *100*, 16082–16086.
- (40) Shvartsburg, A. A.; Jarrold, M. F. An Exact Hard-Spheres Scattering Model for the Mobilities of Polyatomic Ions. *Chem. Phys. Lett.* **1996**, *261*, 86–91.
- (41) Cuendet, M. A.; van Gunsteren, W. F. On the Calculation of Velocity-Dependent Properties in Molecular Dynamics Simulations Using the Leapfrog Integration Algorithm. *J. Chem. Phys.* **2007**, 127, No. 184102.